



Rainfall Infiltration-induced Slope Instability of the Unsaturated Volcanic Residual Soils During Wet Seasons in Indonesia

AGUS SETYO MUNTOHAR¹, JAZAUL IKHSAN¹, HUNG-JIUN LIAO², APINITI JOTISANKASA³, and VICTOR G. JETTEN⁴

¹Department of Civil Engineering, Universitas Muhammadiyah Yogyakarta,
Jln. Brawijaya Tamantirto, Bantul, D.I. Yogyakarta. 55183. Indonesia

²Department of Civil and Construction Engineering, National Taiwan University of Science and Technology,
No. 43 Keelung Rd., Sec. 4, Taipei, 104 Taiwan

³Department of Civil Engineering, Kasetsart University,
50 Thanon Ngamwongwan, Lat Yao, Chatuchak, Bangkok 10900, Thailand

⁴Faculty of Geoinformation Science and Earth Observation (ITC), University of Twente,
Hengelosestraat 99, 7514 AE Enschede, The Netherlands

Corresponding author: muntohar@umy.ac.id

Manuscript received: March, 03, 2020; revised: May, 15, 2020;
approved: June, 21, 2021; available online: January, 7, 2022

Abstract - Located in the ring of fire, Indonesia is widely covered by volcanic soil deposits in various hilly or mountainous areas, especially in Java Island. It is also being characterized as a tropical region, rainfall-induced slope failure in residual volcanic soil, and it is of practical significance to study its mechanism. This paper presents the study of the influence of rainfall and antecedent rainfall pattern on the stability of a residual slope in Yogyakarta. Two residual soil types, clayey sand, SC, and high plasticity clay, CH, were investigated in this study which is of different soil-water and hydraulic characteristics. The studied area was located in Kedungrong Village, Samigaluh, Kulonprogo. The rainfall record was obtained from the automatic rain gauge station in Kalibawang catchment area during November 2001. Two rainfall scenarios were modelled in the numerical analysis; those classified as the major rainfall that precipitates for thirty days (Condition 1) and the three influencing-rainfall (Conditions 2 to 4). Based on the simulation result from the major rainfall and the antecedent rainfall, the slope tended to fail when the precipitation went on continuously for three days with the so-called rolling rainfall pattern. The stability of the slope was dependent on the soil-water and hydraulic properties of the soil layer.

Keywords: rainfall, infiltration, antecedent rain, shallow slope failure, slope stability, residual soil

© IJOG - 2022

How to cite this article:

Muntohar, A.S., Ikhsan, J., Liao, H. J., Jotisankasa, A., and Jetten, V.G., 2022. Rainfall Infiltration-induced Slope Instability of the Unsaturated Volcanic Residual Soils During Wet Seasons in Indonesia. *Indonesian Journal on Geoscience*, 9 (1), p.71-85. DOI: [10.17014/ijog.9.1.71-85](https://doi.org/10.17014/ijog.9.1.71-85)

INTRODUCTION

Background

Indonesia is a tropical country which faces two major problems related to slope stability. High precipitation during the rainy season is the main triggering factor of slope failures. Residual soils cover most slopes in the coun-

try (Tohari *et al.*, 2008). The residual volcanic soils frequently exist in an unsaturated state, since they are commonly situated well above the groundwater table. The unsaturated nature of the residual soils tends to be susceptible to rainfall-induced slope failures (Rahardjo *et al.*, 1995; Muntohar, 2015). In general, slope failures occur most frequently during wet pe-

riods in November to March when there is an increase in moisture content and a decrease in matric suction (Muntohar and Soebowo, 2015). The infiltration from rainfall events into the slope surface causes an increase in porewater pressure, particularly near the surface. Many researches showed that the increase in moisture content would result in a decrease in matric suction and rise in pore water pressure effectively. This condition decreases the shear strength of the soil, making it more susceptible to failure (Rahardjo *et al.*, 2001).

Given that slope failure in tropical residual volcanic soils is widespread, it is of great practical importance to study its mechanism. The mechanism of porewater pressure generation is site-specific; it differs from site to site depending on the hydrological site, rainfall pattern, topography, geology, and soil properties (Johnson and Sitar, 1990; Li *et al.*, 2005; Jotisankasa *et al.*, 2015). Thus, it is necessary to know the specific hydrological response of a soil slope to rainfall to develop a better understanding of the mechanism controlling the initiation of a landslide. The main objectives of this study are to examine the effects of antecedent rainfall on porewater pressure distribution and slope stability. The changes in porewater pressure development pattern due to one-dimensional rainfall infiltration are studied in this paper. In the point of view of a large area, the slope stability is efficiently evaluated based on the analytical or numerical method either simplified 1D method, or 2D, or 3D watershed modelling approaches (Tran *et al.*, 2017; Hen *et al.*, 2020; Ip *et al.*, 2020). However, the last two approaches need some detailed input parameter of the slope (*i.e.* geometry, stratigraphy, topography) and soil properties, including geotechnical and soil-hydraulic properties. Thus, a simplified approach using one-dimensional analysis can be a beneficial tool to analyze a spatial shallow slope failure due to its simplicity (Tran *et al.*, 2017). The 1D or 2D analysis produces more conservative results, but it may be useful for engineering design purpose (Reid *et al.*, 2015; Chen *et al.*, 2020).

One-dimensional Infiltration Model

The one-dimensional Richards equation was solved numerically to simulate water movement in variably saturated media. The fundamental of water movement equation in porous media is described as in Equation (1):

$$\frac{\partial \theta(\psi, t)}{\partial t} = \frac{\partial}{\partial z} \left[K(\psi) \left(\frac{\partial \psi}{\partial z} + \cos \beta \right) \right] \dots\dots\dots (1)$$

In unsaturated-saturated soil, the hydraulic properties, $\theta(\psi)$ and $K(\psi)$, are highly nonlinear functions of the pressure head. The common hydraulic function can be applied using analytical models as written by Genuchten (1980). The model was developed based on the statistical pore-size distribution model of Mualem (1976). The expressions of Vanapalli *et al.* (1996) are given by Equation (3) to (6).

$$\theta(\psi) = \theta_r + (\theta_s - \theta_r) \left[1 + |\alpha \psi|^n \right]^{-m} \dots\dots\dots (2)$$

$$K(\psi) = K_s S_e^l \left[1 - (1 - S_e^{1/m})^m \right]^2 \dots\dots\dots (3)$$

In which

$$S_e = \left[\frac{\theta(\psi) - \theta_r}{\theta_s - \theta_r} \right] \dots\dots\dots (4)$$

$$\text{and } m = 1 - 1/n \dots\dots\dots (5)$$

where:

ψ and θ represent the soil water pressure head and volumetric water content respectively, α corresponds to the air entry value, n represents the slope of SWCC, m is related to the residual water content, t is time, z is vertical coordinate with the origin at the soil surface (positive upward), $K(\psi)$ is the unsaturated hydraulic function, and β is the slope angle.

There were five independent parameters: θ_r , θ_s , α , n , and K_s in the above equations. Jotisankasa and Mairaing (2010) estimated the pore connectivity parameter l in the hydraulic conductivity function was about 0.5 as an average for many soils.

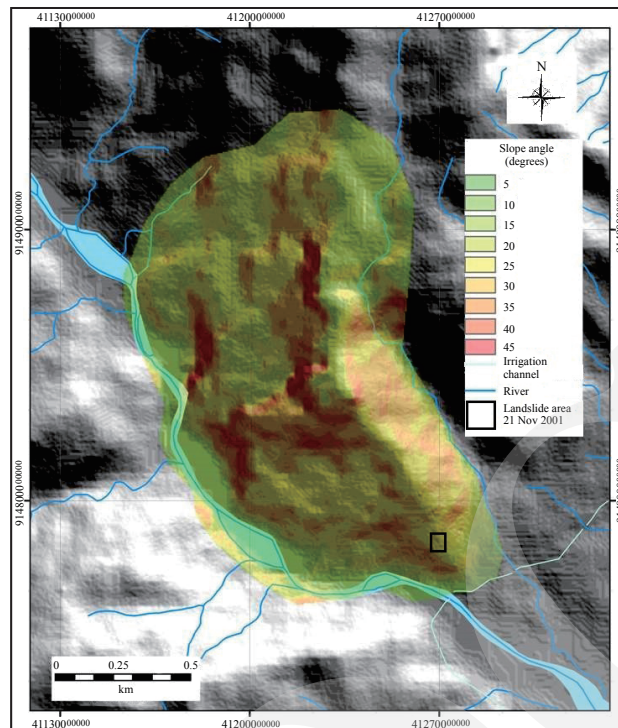


Figure 2. Distribution of slope inclination at the Kedungrong area.

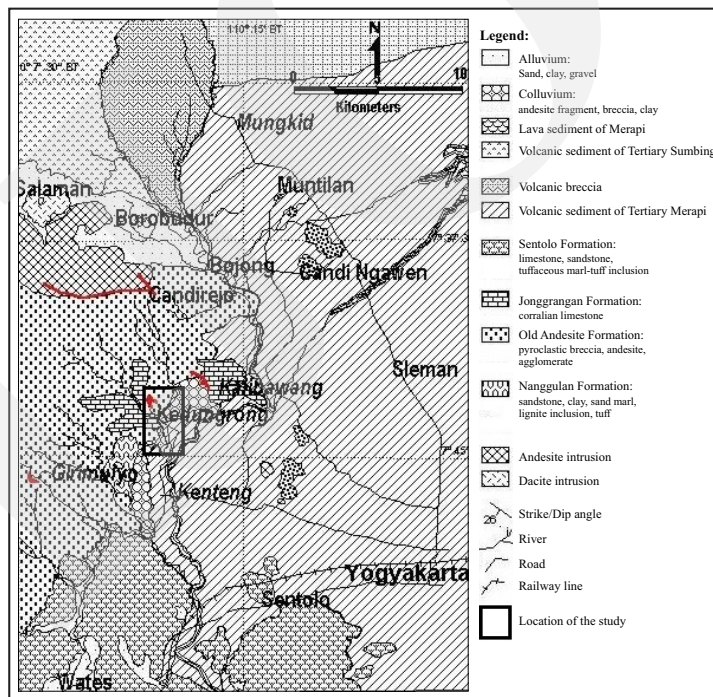


Figure 3. Geological condition of the Kedungrong and adjacent area.

residual soil of weathered breccia. The cohesion of clayey rock ranges from 40 to 70 kPa, and the internal friction angle was 20° - 35°. In comparison, the cohesion of weathered volcanic rock was

25 - 27 kPa, and the friction angle ranged from 20° to 35° (Kusumayudha and Ciptahening, 2016).

This study was aimed at evaluating two slopes covered with two homogeneous residual soil

types. The two soils are identified as the red and black coloured soils. The soil layer was found to be of about 8 m thickness (H). The basic properties of the soils are presented in Table 1. The red soil is thereafter assigned as SC, and black soil is CH, in this paper. Shear strength characteristic of the soils was investigated in the direct shear box. The specimen size was 63.7 mm in diameter and 22 mm in height. A slow multistage-shearing direct shear test was carried out at normal stresses of 31, 62, and 123 kPa to determine the fully saturated shear strength of the soils. The shearing rate was set at 0.05 mm/min such that no excess pore water pressure developed during shearing

Prior to the experiment, a trial saturation test was conducted on the specimen. The specimen was placed in PVC tube and submerged in water batch. The suction was measured by tensiometer hourly, and the specimen weight was measured to determine the water content and degree of saturation. It took approximately 20 hours for the specimen to be fully saturated which was measured by the suction near 10^{-2} kPa. In present study was much less than the trial specimen, after the specimen was placed in shear box bowl, then the specimen was immersed for 24 hours to attain full saturation.

The unsaturated - saturated behaviour of the soils was demonstrated by the soil-water characteristic curve (SWCC). The SWCC was determined using miniature KU tensiometer for suction, ψ , less than 100 kPa, and the filter paper technique for suction, ψ , greater than 100 kPa. The tensiometer apparatus was detailed in Muntohar (2015). The Whatman filter paper No. 42 was used and the suction was inferred using the calibration curve suggested in ASTM D5298 (ASTM, 2013). The schematic apparatus and test-

ing procedures to determined SWCC using filter paper was explained in Muntohar (2015). The SWCC of the soil is shown in Figure 4a. Measurements of unsaturated hydraulic conductivity are timely, difficult to set up and sensitive to error, either in the laboratory on core samples or in the field (Mualem, 1976). It was rendering such measurements impractical for testing field variation. The unsaturated hydraulic conductivity is often obtained from a closed-form mathematical model of SWCC and saturated hydraulic conductivity (k_{sat}), to overcome these difficulties (Doussan and Ruy, 2009; van Genuchten, 1980). The saturated hydraulic conductivity (k_{sat}) of the soil was determined from the double-ring infiltrometer test. The k_{sat} values were 0.0968 m/day and 0.0864 m/day for the SC soil and the CH soil slopes respectively. The measured moisture - suction relationship was fitted using the van Genuchten (1980) model to obtain the SWCC, while the hydraulic conductivity function was predicted using Mualem (1976) model. Figure 4b shows the hydraulic conductivity function of the soils. In this study, the initial suction at the ground surface is measured to be 60 kPa and gradually decreased to zero at the bottom layers at 8 m depth as suggested by Muntohar *et al.* (2013).

Rainfall Scenarios

Figure 5 shows the rainfall hyetograph of the area. The precipitation record was obtained from the automatic rain gauge station in Kalibawang catchment area during November 2001. Slope failures were documented within the rainfall period, on 21 November 2001. According to the criteria proposed by Aleotti (2004) and Hong *et al.* (2018), antecedent rainfall occurred within

Table 1. Properties of the Soil Layer

Parameter	Red Soil (SC)	Black Soil (CH)
Specific gravity, G_s	2.73	
Total unit weight, γ_t	16.1 kN/m ³	17.7 kN/m ³
Particle size:		
Coarse-grained: Gravel/sand	84%	49%
Fine-grained: Silt/clay	16%	51%
Liquid limit, LL	43%	49%
Plasticity index, PI	17%	24%
Soil classification (USCS)	SC	CH
Cohesion (c')	1.7 kPa	9.7 kPa
Internal friction angle (ϕ')	20°	19°
Saturated permeability coefficient (k_{sat})	0.0968 m/day	0.0864 m/day

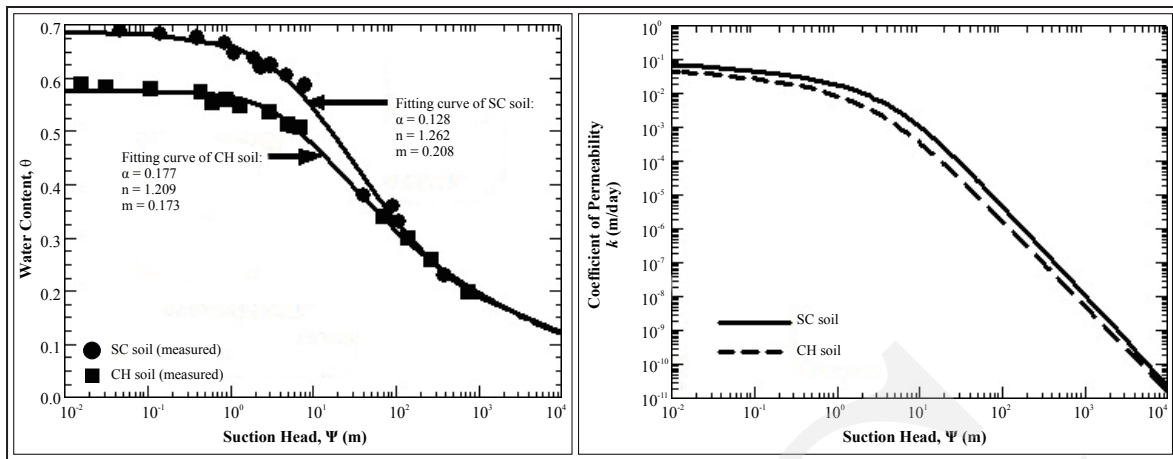


Figure 4. (a) Soil-water characteristic curve, (b) Hydraulic conductivity function of the soil.

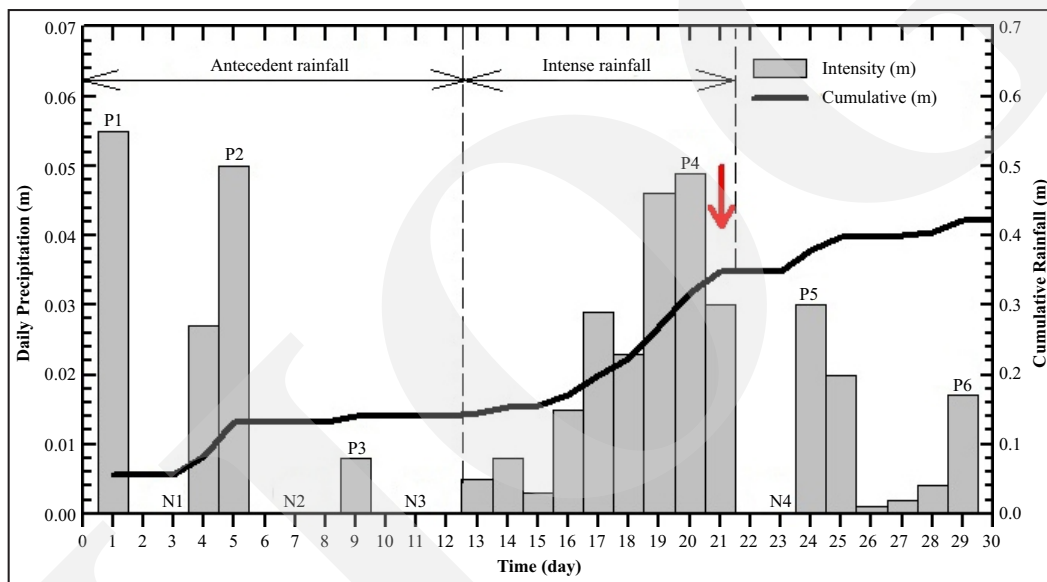


Figure 5. Daily rainfall hyetograph as the major rainfall in the back-analysis.

two weeks prior to the intense or critical rainfall. The transient seepage analysis was divided into three rainfall scenarios. The first case, infiltration analysis was carried out for continuous rainfall within the entire period of analysis, *i.e.* 1st to 30th November 2001. The rainfall was assigned as major rainfall (*Condition 1*). The cumulative rainfall (V_r) was about 0.422 m for 30 days precipitation.

The second rainfall scenario (*Condition 2*) was determined to evaluate the effect of antecedent rainfall on the slope stability. The analysis did not take into account the antecedent precipitation prior the intense rainfall period (see Figure 5). In this research, critical rainfall on 13-21 November

was applied to evaluate the effect of rainfall pattern on slope stability. The total rainfall (V_r) for the period was 0.208 m. Thus, the third scenario, the rainfall was idealized as delayed (*Condition 3*), and average or uniform pattern (*Condition 4*), shown in Figure 6.

RESULTS

Effect of Antecedent Rainfall on the Slope Stability

Figures 7 and 8 provide the results of numerical modelling of the SC and CH slopes under the

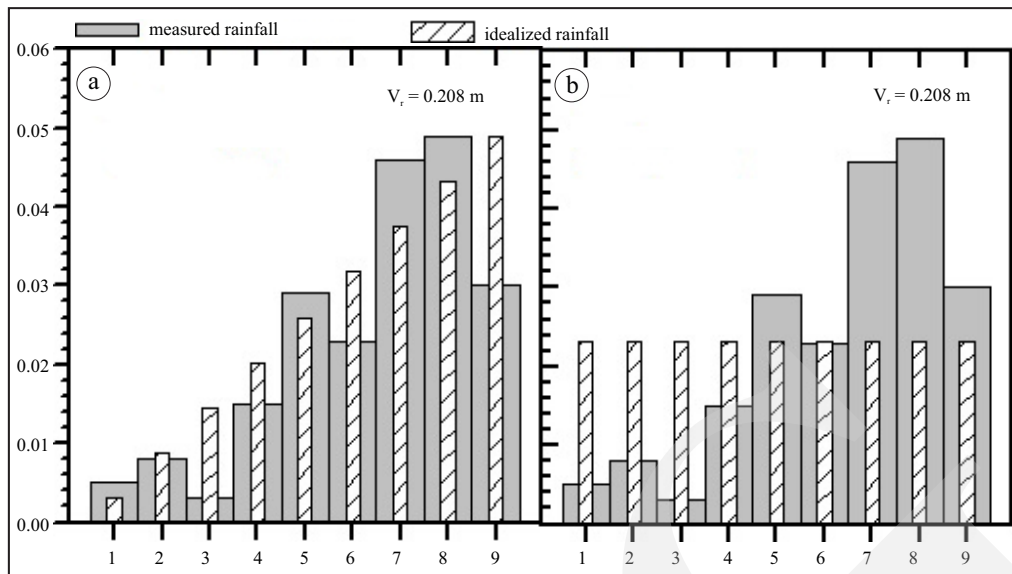


Figure 6. The second rainfall scenarios: (a) condition 3; delayed, (b) condition 4; average (or uniform).

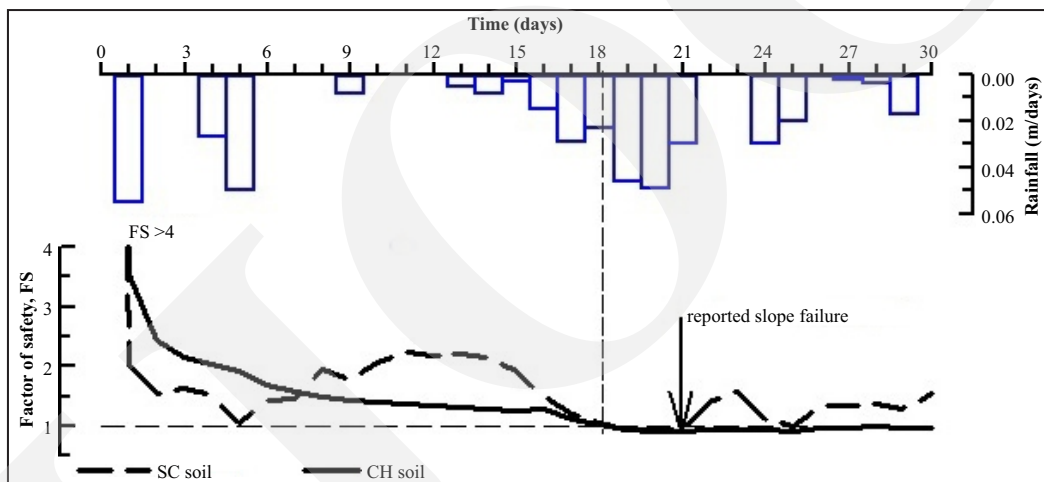


Figure 7. Variation of factor of safety due to Condition 1 rainfall scenarios.

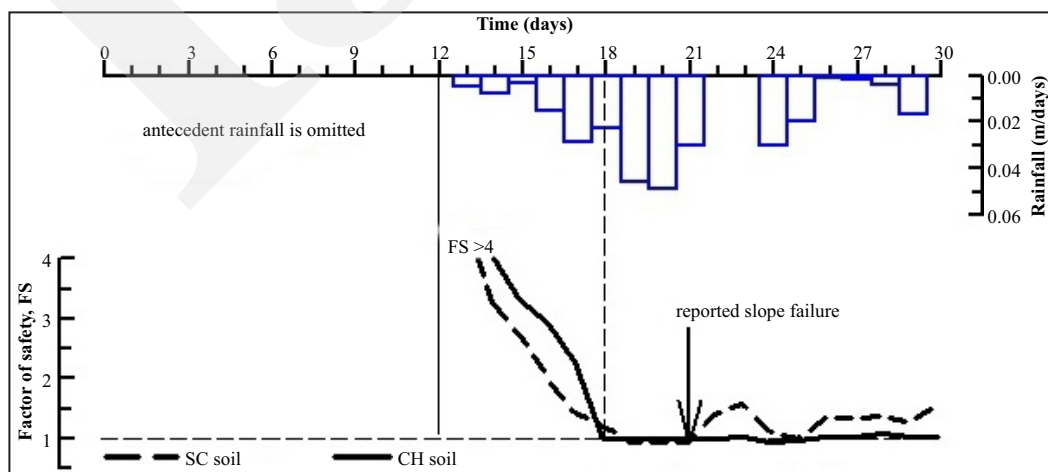


Figure 8. Variation of pore water pressure and factor of safety due to Condition 2 rainfall scenarios.

Condition 1 and Condition 2 rainfall scenarios. The results are displayed in the variation of safety factor (FS) and time (t). Figure 7 accounted for the antecedent rainfall, while it was omitted in Figure 8. In general, the Figures show that the factor of safety varies the rainfall intensities. Both Figures show that the slope is likely stable ($FS > 4$) at the beginning of precipitation and initiate to fail ($FS < 1$) at 18 days. The minimum FS ($FS_{\min} = 0.93$ for SC, and $FS_{\min} = 0.90$ for CH soil) continued to 21 days and days end for SC and CH slopes respectively. The SC slope exhibits a rapid down of the FS during rainfall, and quickly recover when there is no rainfall. This result indicates that the slope with a high k_{sat} value experiences rapid decrease and recover in FS comparable to the slope with a low k_{sat} value. A similar characteristic was concluded by Rahimi *et al.* (2011).

The effect of antecedent rainfall is clearly shown in Figure 8. The FS variation after 18 days is almost similar to the case in Figure 7. The result indicates that the antecedent rainfall does not significantly affect the factor of safety. The antecedent rainfall period was separated by three no-rainfall periods (N1, N2, N3). Prior to the intense rainfall, there were three days no-rainfall period. During the no-rainfall period, the condition leads to increasing the suction at the surface and wetting front. Hence, the effect on the slope stability was insignificant to reduce the factor of safety. Hong *et al.* (2018) explained that if the duration of no-rainfall period was longer than the rainfall event, then the effect of antecedent rainfall was less effective to triggering the landslide. The simulation in Figure 8 is alluding to conclude that the intense rainfall for eight days prior to the landslide event effectively induced slope failure.

The infinite slope model concerns the analysis within the saturation zone where it is located above the wetting front. Thus, the slip surface was potentially located at the wetting front and transitional zone (Duncan and Wright, 1995; Rahardjo *et al.*, 1995). As a consequence of continuous saturation in the wetting front, the factor of safety declines to a value of lesser than one ($FS < 1$) as observed on day 18th to 21st. For the SC

soil, the factor of safety varies with the rainfall intensity. The variation depends on the wetting front and pore water pressure which fluctuated during the rainfall. The reduction and recovery of the factor of safety are higher on SC soil which is comparable in CH soil. It can be contributed to a higher infiltration rate in SC soil than in CH soil, which is affected by the value of parameter “ n ”. Rahimi *et al.* (2010) indicated a soil with a higher value of “ n ” resulting in a higher rate of infiltration, reduction, and recovery in the factor of safety.

Comparison of The Pore Water Pressure Distribution of SC and CH Soils

Figure 9 illustrates the variation of pore water pressure with depth due to major rainfall pattern (Condition 1) for CH and SC soil type, respectively. The Figure shows the pore water pressure response at the selected time at P1 to P6 and N1 to N4 (see Figure 5 for the notation). In general, the Figures demonstrate that the pore water pressure increased with the elapsed time of rainfall depending on the rainfall intensity. At a low rainfall intensity or no rainfall, the wetting front is not clearly defined when the suction at the surface is greater than zero. As the rainfall continuously precipitates the surface, the slope surface becomes saturated. At this condition, then the saturation zone propagates to a deeper layer and form a sharp wetting front (see at P1, P2, and P4). In case of decreases in precipitation or no rainfall event (N1 to N4), the pore water pressure decreased as the result of water redistribution. The model did not take into account the evaporation. Thus, the pore water pressure decreasing at the upper zone is just a result of water redistribution downwards, and no supply of water from the rain above to replenish the soil.

The worst pore water pressure distribution was shown in low permeability soil slope (CH soil). The variation of porewater pressure due to rainfall takes place over a wide range of residual soils with high permeability as compared to residual soils with low permeability. In transient seepage conditions and in response to rainfall, the pore

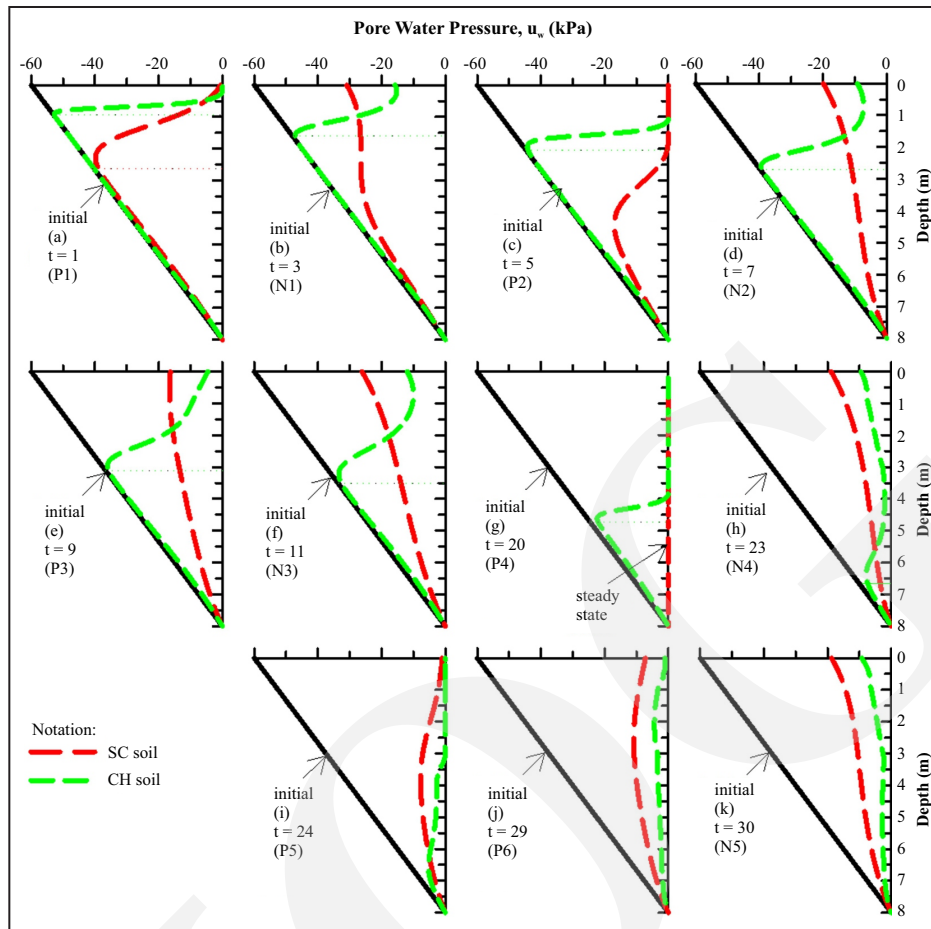


Figure 9. Pore water pressure profile at the major rainfall scenario for CH and SC soils type at the various time of precipitation.

water pressure profile depends on the magnitude of rainfall flux, the saturated coefficient of permeability, and the water storage function. The k_{sat} essentially becomes the upper limit of the infiltration rate, when the ground surface flux under transient conditions is equal to or greater than the saturated coefficient of permeability ($I/k_{sat} \geq 1$). With the same saturated coefficient of permeability, the soil with a larger water storage coefficient has a larger water storage capacity (Kim *et al.*, 2012). Consequently, the downward movement of the wetting front in the soil is slower than that in a soil with a smaller water storage capacity. Given the same water storage function, the matric suction in the soil with a larger saturated coefficient of permeability will disappear more quickly. Some studies recommended the flux ratio (I/k_{sat}) rather than rainfall intensity (I) to investigate the effect of soil hydraulic properties

(Zhang *et al.*, 2004; Rahardjo *et al.*, 2007; Lee *et al.*, 2009). When the I/k_{sat} is higher, the matric suction values at the slope surface decreased and resulted in the decreasing of FS value. The matric suction at slope surface decreases marginally when the I/k_{sat} is greater than 0.3, and slope failure appeared when infiltration flux is very close to the saturated hydraulic conductivity (Zhang *et al.*, 2004; Santoso *et al.*, 2011).

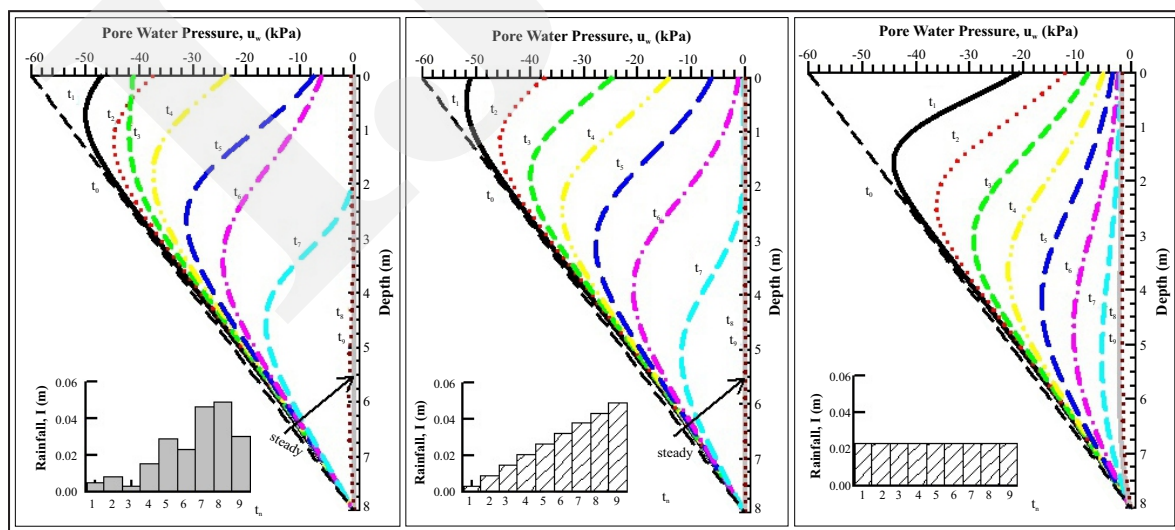
On the response of pore water pressure (see Figure 9), the rainfall infiltrated deeper into the SC soil than the CH soil. However, at this situation, a sharp wetting front is shown more obviously in the CH soil profile. Many researchers, *e.g.* Tsai (2011), Zhai and Rahardjo (2013), Likos and Yao (2014), Rahimi *et al.* (2015), indicated that the shape of the SWCC and hydraulic function generated a difference response in pore water pressure distribution. The shape of SWCC is

determined by the fitting parameter α , n , and m as in Equations (3) and (4). Theoretically, the higher the value of “ α ” the volumetric water content, it will be smaller at the same suction, but the gradient of SWCC will be higher. When the value of “ n ” is smaller, the flow will be faster, less water required to fill the soil for the same amount of suction reduction. However, in this study, the permeability function of the soil plays a greater role than the difference in SWCC. The SC has a higher value of parameter “ α ” than the CH soil. The saturated hydraulic conductivity of the SC soil is greater than the CH soil (see Figure 3b). Rahimi *et al.* (2015) indicated that unsaturated permeability function also controlled the infiltration rate of rainwater into the soil. With respect to the hydraulic conductivity function, a higher permeability function therefore will cause a higher infiltration rate of rainwater into the soil. Then, the rainwater infiltrates more profound into this soil and results in a deeper wetting front.

Effect of The Idealized Rainfall Pattern on The Pore Water Pressure and Slope Stability

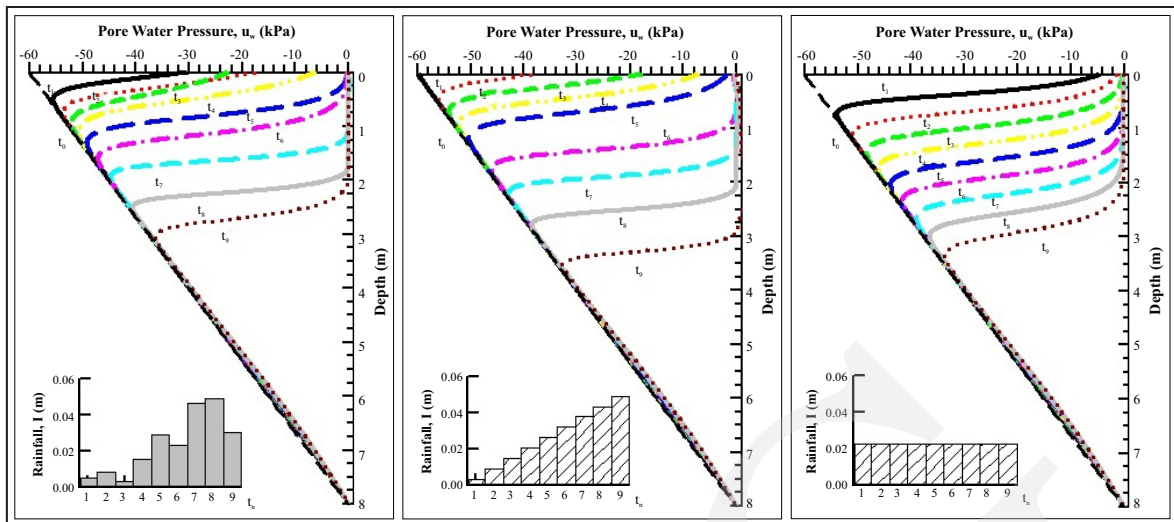
Figures 10 and 11 shows the distribution of pore water pressure for the SC and CH soils under the second rainfall scenario of Condition 3 and 4 rainfall, respectively. Figures 10a and

11a show the pore water pressure distribution of the SC and CH soils under the measured rainfall. Figure 10b shows the pore water pressure distribution associated with the advanced rainfall pattern for the SC slope. The distribution seems similar to the measured rainfall (Figure 10a). When the rainfall was idealized as uniform or average pattern (Figure 10c), the pore water distribution increases drastically from -60 kPa to -22 kPa at the beginning of rainfall (t_1). After eight days of precipitation, the pore water pressure is near to zero ($u_w \propto 0$) at whole soil layers. This condition indicates that the slope is saturated and interferes the slope to become unstable ($FS < 1$, as shown in Figure 12a). The CH soil exhibits different response of pore water pressure (see Figures 11b and 11c). Figure 11b shows the pore water pressure distribution associated with the advanced pattern. The pore water pressure near the slope surface increased from -60 kPa to near zero ($u_w \propto 0$) after six days of rainfall (t_6). The rainwater infiltrated to a deeper soil layer associated with the rainfall duration, and the wetting front is advanced to a 3 m depth at the rainfall end (t_9). A quick decreasing of suction was observed under the uniform rainfall simulation as shown in Figure 11c. The pore water pressure increased from



Note: Time of rainfall $t_1 = 1$ day, $t_2 = 2$ days, ... $t_n = n^{\text{th}}$ days.

Figure 10. Distribution of pore water pressure in SC slope (a). measured rainfall; (b). idealized rainfall Condition 3; and (c). idealized rainfall Condition 4.



Note: Time of rainfall $t_1 = 1$ day, $t_2 = 2$ days, ... $t_n = n^{\text{th}}$ days.

Figure 11. Distribution of pore water pressure in CH slope, (a). measured rainfall; (b). idealized rainfall Condition 3; and (c). idealized rainfall Condition 4.

-60 kPa to -5 kPa after a day of rainfall (t_1) and continued to near zero ($u_w \approx 0$) after three days of rainfall (t_3). The wetting front reached 2 m depth at rainfall end (t_9), which was shallower than the slope under delayed rainfall pattern (see Figure 11b). Kim *et al.* (2012) explained that a soil with a lower hydraulic conductivity and the infiltration distance is comparatively long. It takes more time for water infiltration to reach a higher depth, because water movement on the slope surface in the lower hydraulic conductivity soil is easily delayed compared to the larger one. This result causes the time of slope failure ($FS < 1$) during a uniform rainfall pattern is earlier than the delayed rainfall pattern, as shown in

Figure 12b. This finding was also discussed by Rahimi *et al.* (2011) and Tsai and Wang (2010).

Figure 13 shows the normalized factor of safety to evaluate the rate of the decrease in the factor of safety with the elapsed time of rainfall. The factor of safety at a time t_n , obtained from Figure 12, is divided with the initial factor of safety at time t_0 for corresponding rainfall pattern. Slope subjected to delayed rainfall pattern results in rapid decreasing of the factor of safety. Figure 13 shows that the rainfall patterns influenced the FS reduction rate and the time of failure corresponding to the FS_{min} for both SC and CH soil slopes. The FS of slopes decreased from its initial value by 80 - 82 % under the delayed rainfall pattern, and the FS decreased to

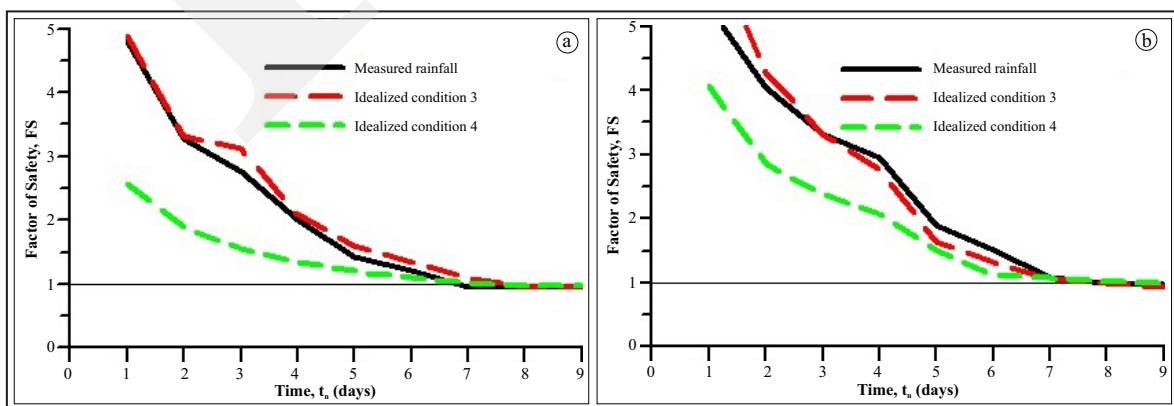


Figure 12. Variation of the factor of safety (FS) with time due to rainfall scenarios, (a). for SC slope; (b). for CH slope.

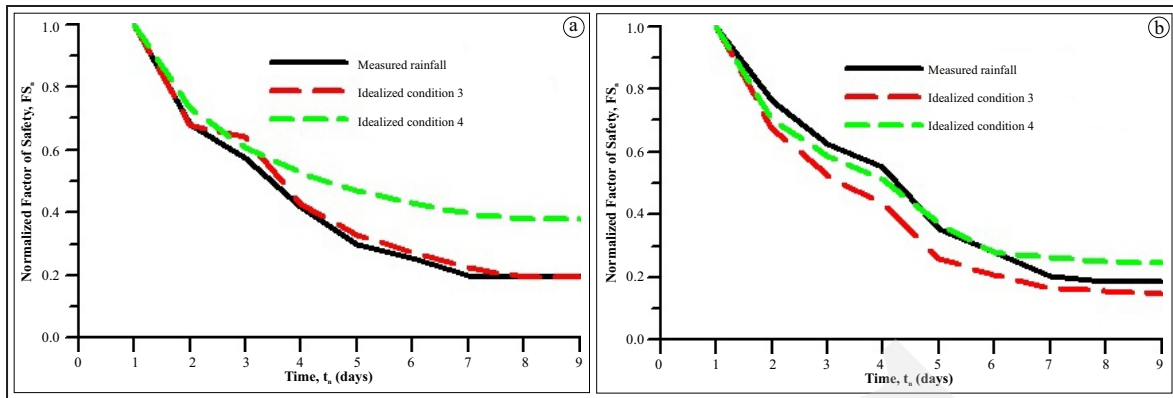


Figure 13. Normalized factor of safety with time due to rainfall scenarios, (a). SC slope; (b). CH slope.

60 - 70 % of its initial value under uniform rainfall pattern. The results show that the FS reduction rate of CH slope (Figure 13b) is higher than the SC slope (Figure 13a).

Application of The Rainfall and Infiltration-Slope Stability Model

Hourly rainfall was recorded from January 1998 to December 2015 (Figure 14). Landslides often occur during the wet season from Novem-

ber to April (Muntohar and Ikhsan, 2015). The rainfall duration in a day and the daily rainfall intensity of each month from November to April is shown in Table 2. The idealized average rainfall (Condition 4) produces the worst factor of safety. Then, the model can be adapted to predict the slope instability during the wet season. The summary of the factor of safety for each month is presented in Table 3. The slope achieves the worst stability in December, which the factor of

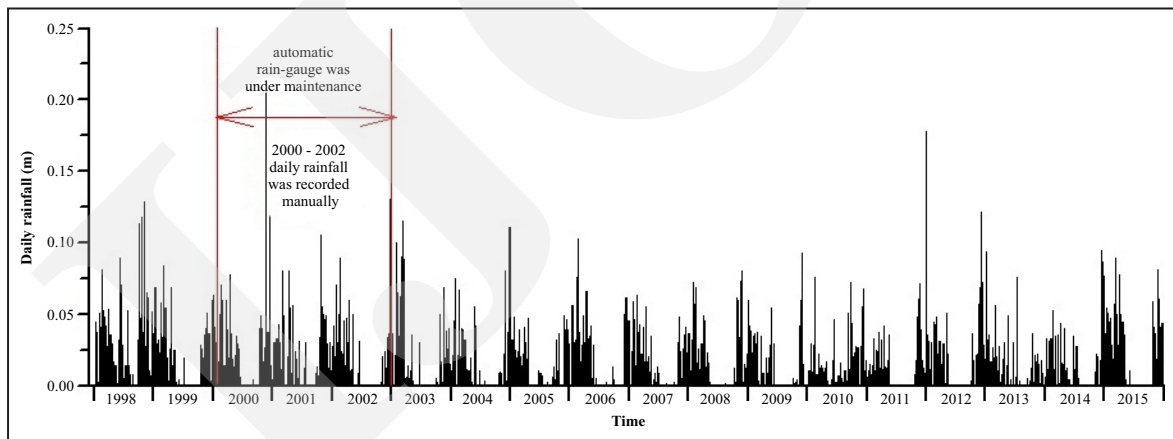


Figure 14. Precipitation distribution from January 1998 to December 2015 in Kalibawang rainfall station.

Table 2. Properties of Rainfall from 1998 - 2015 and Factor of Safety During Wet Season

Month	Average day of precipitation \bar{x}_d (day)	Average Daily Rainfall \bar{x}_r (mm)	Minimum Factor of Safety, FS_{min}	
			CH soil	SC soil
November	8	0.0166	1.13	1.21
December	9	0.0157	1.12	1.17
January	8	0.0145	1.21	1.37
February	9	0.0152	1.14	1.24
March	8	0.0142	1.23	1.39
April	7	0.0120	1.33	1.78

safety is the lowest during the rainy season of November - April. The slope covered by CH soil experiences a lower factor of safety compared to the slope with SC soil. The result is consistent with the analysis in Figure 13.

CONCLUSIONS

This paper investigated the mechanisms of rainfall-induced slope failure in the Kedung-rong area, Indonesia, through a numerical simulation. The study investigated the effect of selected rainfall characteristics and soil type. The simulation results conclude that the slope failure may not necessarily be triggered by a major rainfall event that occurred on the whole month. A prolonged antecedent rainfall plays a role in triggering the failure of the slope. The slope failure would potentially occur when rainfall continuously precipitates on the slope surface for about three days. This condition resulted in continuous saturation on the wetting front. The characteristics of the saturated-unsaturated function of the residual soil affected the destabilization pattern of the slope. Thus, understanding and determination of the saturated-unsaturated function is significant to study the mechanism of the slope failure. Under the delayed rainfall pattern, the FS of slope decreased by 80 - 82 % from its initial value, and the soil slopes of FS decreased to 60 - 70 % of its initial value under uniform rainfall patterns. A uniform or average rainfall pattern has been commonly and easily used to evaluate the slope stability. The slope covered by soil with a low hydraulic conductivity experience a lower factor of safety compared to the slope with high hydraulic conductivity.

ACKNOWLEDGMENT

This research was fully funded by the Ministry of Research, Technology, and Higher Education, the Republic of Indonesia through

number grant DIPA-042.06.0.1.401516/2016 in 2015-2016 and contract number 227/SP2H/LT/DRPM/2019 in 2019-2021. The support from Universitas Muhammadiyah Yogyakarta through "International-Collaborative Research" grant is highly appreciated to make this research viable and effective.

REFERENCES

- Aleotti, P., 2004. A warning system for rainfall-induced shallow failures. *Engineering Geology*, 73, p.247-265. DOI:10.1016/j.eng-geo.2004.01.007
- ASTM, 2013. Standard Test Method for Measurement of Soil Potential (Suction) Using Filter Paper. *In*: West Conshohocken, Pennsylvania, USA: ASTM International.
- Chen, L.K., Chang, C.H., Liu, C.H., and Ho, J.Y., 2020. Application of a Three-Dimensional Deterministic Model to Assess Potential Landslides, a Case Study: Antong Hot Spring Area in Hualien, Taiwan. *Water*, 12 (2). DOI:10.3390/w12020480
- Doussan, C. and Ruy, S., 2009. Prediction of unsaturated soil hydraulic conductivity with electrical conductivity. *Water Resources Research*, 45 (10). DOI:10.1029/2008wr007309
- Duncan, J.M. and Wright, S.G., 1995. *Soil Strength and Slope Stability*. Hoboken, NJ, USA: Wiley.
- Fredlund, D., Morgenstern, N. R., and Widger, R., 1978. The shear strength of unsaturated soils. *Canadian Geotechnical Journal*, 15 (3), p.313-321.
- Hong, M., Kim, J., and Jeong, S., 2018. Rainfall Intensity-Duration Thresholds for Landslide Prediction in South Korea by Considering The Effects of Antecedent Rainfall. *Landslides*, 15 (3), p.523-534. DOI:10.1007/s10346-017-0892-x.
- Ip, S.C.Y., Rahardjo, H., and Satyanaga, A., 2020. Three-dimensional slope stability analysis incorporating unsaturated soil properties in Singapore. *Georisk: Assessment and Manage-*

- ment of Risk for Engineered Systems and Geohazards*, p.1-15. DOI:10.1080/1749951.2020.1737880
- Johnson, K.A. and Sitar, N., 1990. Hydrologic Conditions Leading to Debris-Flow Initiation. *Canadian Geotechnical Journal*, 27 (6), p.789-801.
- Jotisankasa, A., Mahannopkul, K., and Sawangsurinya, A., 2015. Slope Stability and Pore-Water Pressure Regime in Response to Rainfall a Case Study of Granitic Fill Slope in Northern Thailand. *Geotechnical Engineering Journal of the SEAGS & AGSSEA*, 46 (1), p.45-54.
- Jotisankasa, A. and Mairaing, W., 2010. Suction-Monitored Direct Shear Testing of Residual Soils from Landslide-Prone Areas. *Journal of Geotechnical and Geoenvironmental Engineering*, 136 (3), p.533-537. DOI:10.1061/(ASCE)GT.1943-5606.0000225.
- Kim, J., Jeong, S., and Regueiro, R.A., 2012. Instability of Partially Saturated Soil Slopes Due To Alteration of Rainfall Pattern. *Engineering Geology*, 147-148, p.28-36. DOI:10.1016/j.enggeo.2012.07.005.
- Kusumayudha, S.B. and Ciptahening, A.N., 2016. Correlation between Tectonic Environment and Characteristics of Mass Movement (Landslides): A Case Study from Java, Indonesia. *Journal of Geological Resource and Engineering*, 4 (2). DOI:10.17265/2328-2193/2016.02.001.
- Lee, L.M., Gofar, N., and Rahardjo, H., 2009. A simple model for preliminary evaluation of rainfall-induced slope instability. *Engineering Geology*, 108 (3-4), p.272-285. DOI:10.1016/j.enggeo.2009.06.011.
- Li, A.G., Yue, Z.Q., Tham, L.G., Lee, C.F., and Law, K.T., 2005. Field-Monitored Variations of Soil Moisture and Matric Suction in A Saprolite Slope. *Canadian Geotechnical Journal*, 42 (1), p.13-26. DOI:10.1139/t04-069.
- Likos, W.J. and Yao, J., 2014. Effects of Constraints on van Genuchten Parameters for Modeling Soil-Water Characteristic Curves. *Journal of Geotechnical and Geoenvironmental Engineering*, 140 (12), 06014013-06014011. DOI:10.1061/(ASCE)GT.1943-5606.0001168.
- Mualem, Y., 1976. A New Model for Predicting the Hydraulic Conductivity of Unsaturated Porous Media. *Water Resources Research*, 12 (3), p.513-522. DOI:10.1029/WR012i003p00513.
- Muntohar, A. S., 2015. *Influence of the Soil-Water Retention Curve Models on the Stability of Residual Soils Slope*. In: Prakoso, W.A., Jitno, H., Hutapea, B.M., and Djarwadi, D., (Ed.), *Pertemuan Ilmiah Tahunan ke-19 Himpunan Ahli Teknik Tanah Indonesia*, Jakarta, Indonesia, 24-25 November 2015, p.237-244
- Muntohar, A.S. and Ikhsan, J., 2015. *A Study on the effect of climate change on slope instability*. Research Report to Ministry of Research, Technology, and Higher Education: Universitas Muhammadiyah Yogyakarta (in Indonesia).
- Muntohar, A.S., Ikhsan, J., and Soebowo, E., 2013. Mechanism of rainfall triggering landslides in Kulonprogo, Indonesia. In: Meehan, C.L., Pradel, D., Pando, M.A., and Labuz, J.F., (Eds.), *Geo-Congress 2013*. American Society of Civil Engineers, San Diego, California, pp. 452-461. DOI: 10.1061/9780784412787.047
- Muntohar, A.S. and Soebowo, E., 2015. *Stability Analysis of A Shallow Slope Failure During Rainy Season In Kulonprogo, Indonesia*. In: Rahardjo, P.P. and Tohari, A. (Eds.), *International Conference On Landslides and Slope Stability (SLOPE 2015)*, Bali, Indonesia, 27-30 September 2015, F5.1-F5.8
- Rahardjo, H., Li, X.W., Toll, D.G., and Leong, E.C., 2001. The Effect of Antecedent Rainfall on Slope Stability. *Geotechnical and Geological Engineering*, 19, p.371-399.
- Rahardjo, H., Lim, T.T., Chang, M.F., and Fredlund, D.G., 1995. Shear-Strength Characteristics of A Residual Soil. *Canadian Geotechnical Journal*, 32, p.60-77.
- Rahardjo, H., Ong, T.H., Rezaur, R.B., and Leong, E.C., 2007. Factors Controlling Instability of Homogeneous Soil Slopes Under Rainfall. *Journal of Geotechnical and Geoenvironmental Engineering*, 133 (12), p.1532-1543. DOI:10.1061/(ASCE)1090-

- 0241(2007)133:12(1532).
- Rahimi, A., Rahardjo, H., and Leong, E.C., 2010. Effect of Hydraulic Properties of Soil on Rainfall-Induced Slope Failure. *Engineering Geology*, 114, p.135-143.
- Rahimi, A., Rahardjo, H., and Leong, E.C., 2011. Effect of Antecedent Rainfall Patterns on Rainfall-Induced Slope Failure. *Journal of Geotechnical and Geoenvironmental Engineering*, 137 (5), p.483-491. DOI:10.1061/(ASCE)GT.
- Rahimi, A., Rahardjo, H., and Leong, E.C., 2015. Effect of range of soil - water characteristic curve measurements on estimation of permeability function. *Engineering Geology*, 185, p.96-104.
- Reid, M.E., Christian, S.B., Brien, D.L., and Henderson, S.T., 2015. *Scoops3D-Software to Analyze Three-Dimensional Slope Stability Throughout a Digital Landscape*. Reston, Virginia: U.S. Geological Survey.
- Santoso, A.M., Phoon, K.-K., and Quek, S.-T., 2011. *Effect of 1D Infiltration Assumption on Stability of Spatially Variable Slope*. In: Juang, C.H., Phoon, K.K., Puppala, A.J., Green, R.A., and Fenton, G.A., (Eds.), *GeoRisk 2011: Geotechnical Risk Assessment and Management*, Atlanta, Georgia, United States, June 26-28 2011, p.704-711.
- Tohari, A., Sarah, D., and Daryono, M.R., 2008. Hydrological Condition Leading to Landslide Initiation. *Media Teknik Sipil*, 8 (2), p.67-76.
- Tran, T.V., Alvioli, M., Lee, G., and An, H.U., 2017. Three-dimensional, time-dependent modeling of rainfall-induced landslides over a digital landscape: a case study. *Landslides*, 15 (6), p.1071-1084. DOI:10.1007/s10346-017-0931-7.
- Tsai, T.L., 2011. Influences of soil water characteristic curve on rainfall-induced shallow landslides. *Environmental Earth Sciences*, 64, p.449-459. DOI:10.1007/s12665-010-0868-9.
- Tsai, T.L. and Wang, J.K., 2010. Examination of influences of rainfall patterns on shallow landslides due to dissipation of matric suction. *Environmental Earth Sciences*, 63 (1), p.65-75. DOI:10.1007/s12665-010-0669-1.
- Van Genuchten, M.T., 1980. A Closed-Form Equation for Predicting the Hydraulic Conductivity of Unsaturated Soils. *Soil Science Society of American Journal*, 44, p.892-898.
- Vanapalli, S.K., Fredlund, D.G., Pufahl, D.E., and Clifton, A.W., 1996. Model for the prediction of shear strength with respect to soil suction. *Canadian Geotechnical Journal*, 33, p.379-392.
- Zhai, Q. and Rahardjo, H., 2013. Quantification of uncertainties in soil-water characteristic curve associated with fitting parameters. *Engineering Geology*, 163, p.144-152. DOI:10.1016/j.enggeo.2013.05.014.
- Zhang, L.L., Fredlund, D.G., Zhang, L.M., and Tang, W.H., 2004. Numerical Study of Soil Conditions Under Which Matric Suction Can Be Maintained. *Canadian Geotechnical Journal*, 41 (4), p.569-582. DOI:10.1139/t04-006.